

Long columnar defects with constant column size in 180-MeV Fe-irradiated $\text{Bi}_2\text{Sr}_2\text{CaCu}_2\text{O}_x$ crystals

Daxiang Huang* and Yukichi Sasaki

Japan Fine Ceramics Center, 2-4-1 Mutsuno, Atsuta-ku, Nagoya 456-8587, Japan

Izumi Hirabayashi

Superconductivity Research Laboratory, ISTE, 2-4-1 Mutsuno, Atsuta-ku, Nagoya 456-8785, Japan

Yuichi Ikuhara

Department of Materials Science, University of Tokyo, Tokyo 113, Japan

(Received 19 April 1999; revised manuscript received 2 February 2000)

180-MeV Fe ion beams were used to bombard the $\text{Bi}_2\text{Sr}_2\text{CaCu}_2\text{O}_x$ single crystals. The damage morphologies along the ion traces were investigated using cross-sectional transmission electron microscopy. Comparing with heavy-ion (Au or Pb) irradiation, the light Fe-ion irradiation shows several specific damage behaviors: the appearance of long columnar defects with constant column size, the disappearance of the peak of damage efficiency, and the much lower threshold of stopping power for generating columnar defects. An effective method has been developed for qualitatively analyzing the changing law of the damage size with the ion velocity. The applications on both Fe- and Au-irradiated $\text{Bi}_2\text{Sr}_2\text{CaCu}_2\text{O}_x$ crystals and the obtained results indicate that the appearance of long columnar defects with constant column size is a specific phenomenon only occurring in light-ion irradiation. A qualitative analysis has been also done to prove that the threshold of stopping power for generating columnar defects is not a material constant but decreases as the mass of incident ion decreases, which further explains the lower threshold of stopping power in light Fe-ion irradiation.

I. INTRODUCTION

Ion irradiation has been widely used to artificially introduce some specific defect structures in target materials for modifying the physical properties of target materials. For example, in oxide superconducting materials, the defects induced by ion irradiation can strongly pin flux and enhance the critical current density (J_c) to about two orders of magnitude.¹⁻¹² In order to understand the mechanisms for such kinds of irradiation-induced changes of physical properties, first we have to have a good understanding for the evolution of irradiation damage in target materials.

It is known that the degree of irradiation damage strongly depends on the stopping power (dE/dx) of the incident ion in the target, the ion velocity, the crystallographic orientation of target to the incident ion, the stoichiometry of the target, the perfection of the target crystal, and the thermal conductivity of the target material as well.¹⁰ Since there are so many influence factors, it is very difficult to understand the forming conditions of irradiation damage, as well as the detailed influence of any factor on the irradiation damage process.

However, it can be found that most of the influence factors are related to the species of incident ion and the properties of the detailed target material. That is to say, if fixing the ion species and the target material to discuss the irradiation damage in the single ion-target irradiation system, things will become much more simple. In this case, most of the influence factors can be treated as constants. The number of changeable influence factors will be decreased to only 2: the ion velocity and the ion effective charge. Then, the forming conditions of irradiation damage can be fully understood through clarifying the detailed influences of these two

changeable factors on irradiation damage process.

Recently, we have introduced a cross-sectional observation method¹² to measure the damage size continuously along the ion trace, which enables us to analyze the irradiation damage process in a single ion-target system. Later, an effective method has been further established for analyzing the detailed influence of ion velocity on the damage process.¹³ The application on the Au- $\text{Bi}_2\text{Sr}_2\text{CaCu}_2\text{O}_x$ irradiation system shows that there is a critical velocity at which the damage efficiency is maximum. Interestingly, in the comparing analysis for the existent irradiation data in the target of yttrium garnet, we found that the changing law of damage efficiency with ion velocity in light-ion irradiation is much different from that in heavy-ion irradiation.¹³ For the same ion velocity, the damage efficiency is much lower in the light-ion irradiation than in the heavy-ion irradiation, indicating the existence of some specific damage behaviors in light-ion irradiation.

In this study, we focus on the damage process in light-ion irradiation. Instead of heavy Au- or Pb-ion beams, we used relatively light Fe-ion beams to bombard $\text{Bi}_2\text{Sr}_2\text{CaCu}_2\text{O}_x$ single crystals. The same methods suggested in Refs. 12 and 13 have been used for analyzing the evolution of irradiation damage along the ion trace and the velocity dependence of damage efficiency in Fe- $\text{Bi}_2\text{Sr}_2\text{CaCu}_2\text{O}_x$ irradiation system. A similar changing law of damage morphology as in Au- $\text{Bi}_2\text{Sr}_2\text{CaCu}_2\text{O}_x$ irradiation system¹² has been observed along the ion trace. Differing from the decreasing damage size along the ion trace in heavy Au-ion irradiation, the columnar defect size in Fe irradiation almost keeps a constant in a large ion-penetration-depth region. Also, it is surprised that a critical velocity, which usually appeared in heavy-ion

irradiation, does not exist in light Fe irradiation. The threshold of dE/dx for producing columnar defects in Fe irradiation was found to be much lower than that in heavy-ion irradiation. Then, some theoretical analyses have been done for explaining the formation of the long columnar defects with uniform column size. Finally, a brief explanation has been given for the lower dE/dx threshold for producing visible columnar defects in light Fe irradiation.

II. EXPERIMENTS

The $\text{Bi}_2\text{Sr}_2\text{CaCu}_2\text{O}_x$ bulk samples prepared by the floating-zone melting method¹⁴ were used as the target material in the present irradiation experiments. Before the ion irradiation the bulk samples were firstly cleaved into crystal sheets with a thickness of several tens of micrometers along the a - b plane by a scalpel. Subsequently, the crystal sheets obtained were further cleaved using stick tape to reach a smooth sample surface and a suitable sample thickness. In the present experiments, the sample thickness was controlled to be about $25 \mu\text{m}$ according to the estimated penetration range of incident ions in the target material. The final cleaved thin crystal sheets were then cut to a size of $1 \times 2 \text{ mm}^2$ along a and b axis for the ion irradiation experiments.

180-MeV Fe-ion beams were used to irradiate the $\text{Bi}_2\text{Sr}_2\text{CaCu}_2\text{O}_x$ thin sheets at room temperature. The incident Fe^{8+} ions were produced in a Tandem accelerator at the Japan Atomic Energy Research Institute. The incident direction of the ion beams was along the c direction (perpendicular to the surface of the thin crystal sheet). The used ion dose was about 3.3×10^{11} ions/ cm^2 . The depth profile of dE/dx was calculated using a high-energy-extended EDEP-1 code.¹⁵

The damage sizes for the incident ions at different penetration depths were measured by using a cross-sectional TEM observation method, which was reported by the authors in Ref. 12. Damage efficiency (ε), as one of the main parameters used in this study, is defined through relation $\varepsilon = A/(dE/dx)$, for describing the relation of the damage cross section (A) with the stopping power (dE/dx). For analyzing the velocity dependence of damage efficiency, the

method suggested in Ref. 13 has been used.

In the cross-sectional sample preparation, one irradiated $\text{Bi}_2\text{Sr}_2\text{CaCu}_2\text{O}_x$ thin crystal sheet was sandwiched between two silicon pellets and pasted them together by Gatan G1 glue. Perpendicular to the surface of specimen (a - b plane), the pasted specimen was cut into slices along the a or b axis of the crystal. The slices were then mechanically polished to about $50 \mu\text{m}$, dimpled to about $10 \mu\text{m}$, and finally ion milled with a liquid-nitrogen cold stage. The prepared cross-sectional specimens were examined using a Topcon EM-002B high-resolution TEM.

III. RESULTS AND DISCUSSIONS

A. Changes of damage morphology and columnar defect size along the ion traces

Figure 1 gives a series of bright-field TEM images taken in different penetration depth regions in 180-MeV Fe-irradiated $\text{Bi}_2\text{Sr}_2\text{CaCu}_2\text{O}_x$ crystals, showing the change of the irradiation-damage morphology along the ion traces. Similar to the reported results in the 230-MeV Au-irradiation case,¹² the irradiation-damage morphology appears first as only parallel columnar defects when the ion energy is very high. As the incident ion moving in the target and losing its energy gradually, we can find some columnar defects deflected in a large angle due to the strong nuclear collisions of the high-energy ions with some target atoms. In this case, the irradiation-damage morphology will appear as many parallel columnar defects mixed with some large-angle-deflected columnar defects. As the ion energy decreases further, the density of such large-angle-deflected columnar defects becomes higher and higher. When the ion energy decreases to some specific value, then we can find that some cascade defects, distributing in order along the columnar defects, are generated to form another specific damage morphology: cascade-defect-dotted columnar defects. Later, as the ion energy become lower and lower, the damage morphology will change to be ordered cascade defects and finally disordered cascade defects. The distributed depth region and the generation conditions, such as the required ion energy and dE/dx , for these

TABLE I. Regions of ion penetration depth, ion energy, and stopping power for generating five kinds of defect morphologies in Fe-irradiated $\text{Bi}_2\text{Sr}_2\text{CaCu}_2\text{O}_x$ crystals.

Depth (μm)	0	→	6	→	11	→	13.5	→	16	→	18.5
Fe-ion energy (MeV)	180	→	108	→	48	→	22	→	5.1	→	0.6
Stopping power (keV/nm)	11.7	→	12.3	→	11.3	→	9	→	3.9	→	0.08
Parallel columnar defects		●		●		●					
Large-angle-deflected columnar defects				●		●					
Ordered cascade defects						●		●			
Disordered cascade defects											●
Morphologies of irradiation damage		pure paral. col. def.		mixed col. def.		cas.-dotted col. def.		ordered cas. def.			disordered cas. def.

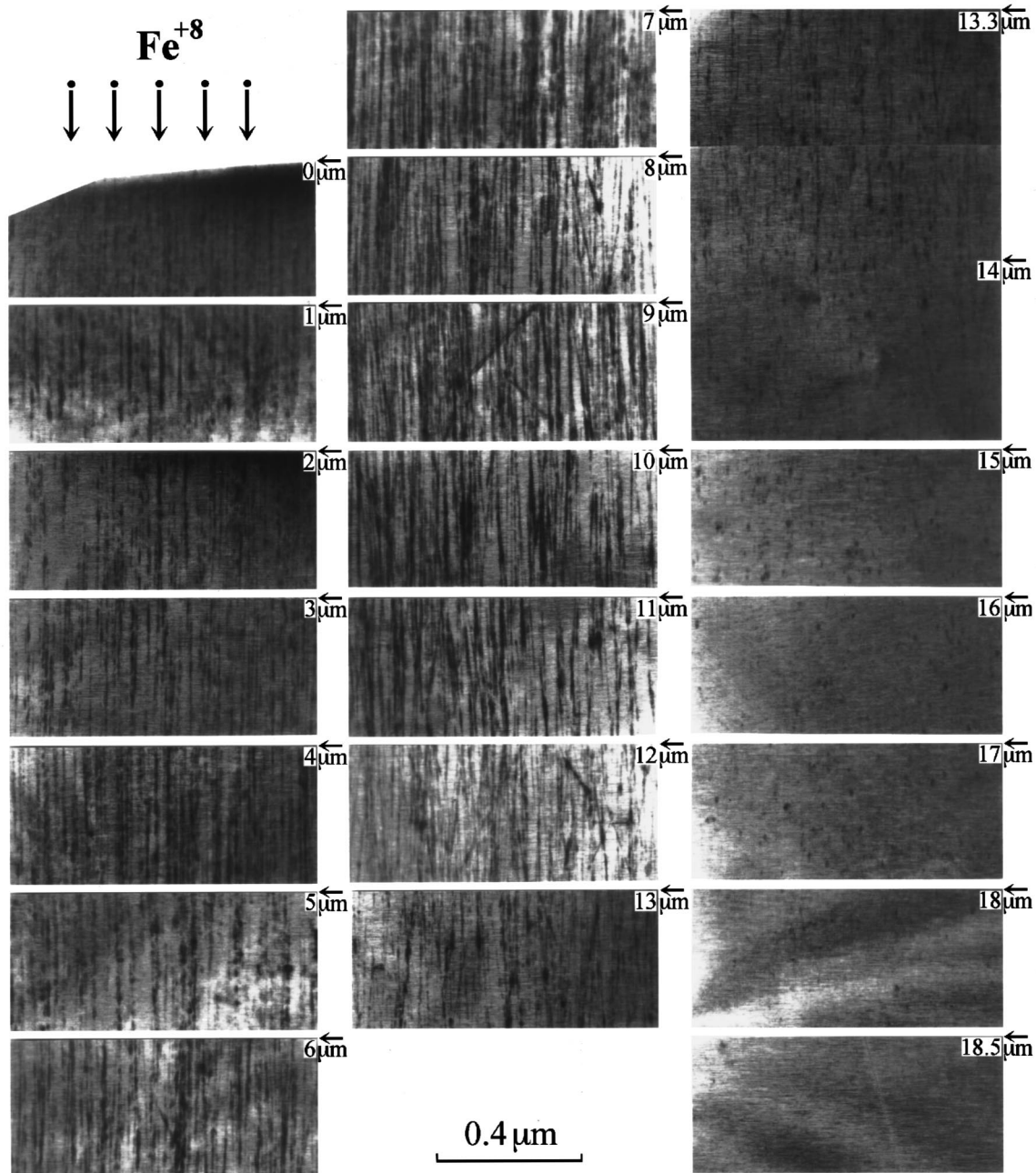


FIG. 1. A series of bright-field images picked out at an equal distance from the images continuously taken along the ion path. The arrow located at the right side of each image shows the detailed ion penetration depth.

five kinds of irradiation-damage morphologies have been estimated and shown in Table I.

Usually, in the cases of heavy-ion irradiation, the produced columnar defect size decreases as the incident ion penetrates the target crystal and loses its energy gradually.¹² In the case of light Fe-ion irradiation, however, the columnar defect size was found to be almost a constant in a large penetration depth region from the bombarded surface to the depth of about 13.5 μm . Figures 2(a)–(c) are the high-resolution electron microscopy (HREM) images respectively taken at the ion-penetration depths of about 0.5 (around surface), 6, and 13.5 μm , showing the similar size of columnar defect in three very different regions of penetration depth. The detailed distribution of the columnar defect size against the ion penetration depth is shown by Fig. 3. In the whole

ion penetration path, we can see that the columnar defect size is almost uniform with a value of ~ 1.5 nm in radius. Table II gives a summary of ion energy, ion velocity, stopping power, measured and calculated radii of columnar defect, and damage efficiency in each penetration depth region.

B. Velocity dependence of damage efficiency

Similar to the Au irradiation case, the velocity dependence of damage efficiency was also analyzed in light Fe-irradiated $\text{Bi}_2\text{Sr}_2\text{CaCu}_2\text{O}_x$ crystals. The detailed data were already shown in Table II. As a comparison, the damage efficiency-velocity (ϵ - v) curve has been drawn together with two published ϵ - v curves in the heavy-ion irradiation cases and all the curves are shown by Fig. 4. It can be found

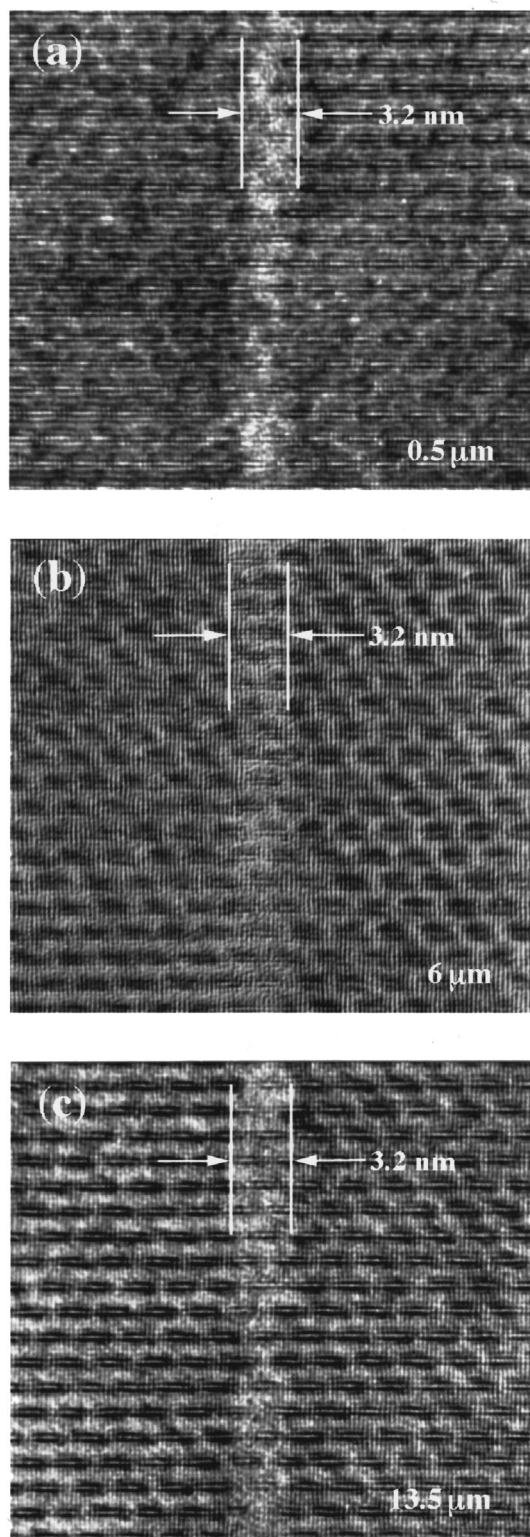


FIG. 2. HREM images respectively taken at penetration depths of about (a) $0.5 \mu\text{m}$, (b) $6 \mu\text{m}$, and (c) $13.5 \mu\text{m}$ along the ion path, showing the columnar defect sizes in different ion penetration depth regions.

that the peak of damage efficiency, usually existing in the low velocity region in the cases of heavy-ion irradiation, does not appear in the light Fe-ion irradiation case. Instead, on the ε - v curve, there is a long plateau of damage efficiency appeared in a large region of ion velocity.

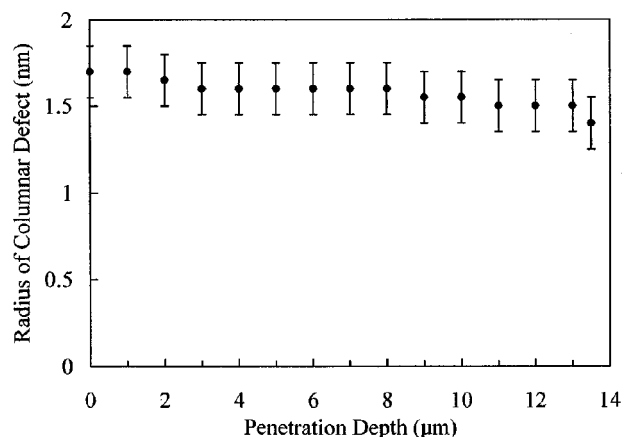


FIG. 3. The distribution of the columnar defect size with the ion penetration depth in 180-MeV Fe-irradiated $\text{Bi}_2\text{Sr}_2\text{CaCu}_2\text{O}_x$ crystals. The error bar gives the real distribution region for the columnar defect size in each ion penetration depth region.

C. Analysis of the changing law of damage size along the ion traces

1. A suggested method

Since the discovery of the strong dependence of irradiation damage on ion velocity,^{13,16–18} it has been known that the most commonly used parameter, stopping power (dE/dx), is not a suitable one for describing the damage degree in the ion-irradiated materials. Since then, all the researchers in this field have had to face a challenge for redefining some other suitable parameters to describe the damage degree. Even though some attempts have already made by Studer, Meftah, and co-workers,^{18–21} unfortunately some shortages still exist in all the defined parameters.

Here we suggest a method to estimate the damage degree, especially the changing law of damage size along the ion trace. In this method, two kinds of parameters have been used. One is the radial distribution curve of the deposited energy density, $D(r)$ - r curve. The second is the minimum value of deposited energy density for producing permanent damage in the target material D_0 . For a given ion-target system, we can calculate the radial distribution of the deposited energy density $D(r)$ for the ion with a given velocity by using the method suggested by Zhang²² and Waligórski, Hamm, and Katz.²³ When D_0 , as a material constant, is known, from the $D(r)$ - r curve we can find a value of r , r_0 , at which the corresponding $D(r_0)$ equals D_0 . When the value of r is larger than r_0 , the value of $D(r)$ will be less than D_0 . This means that no permanent damage will be produced in the area where the radial distance from the ion path is larger than r_0 . Therefore, theoretically, r_0 should correspond to the damage radius of the incident ion in the target material. For the ion with a changing velocity along the ion path, similarly, we can calculate a series of $D(r)$ - r curves. Then, a series of damage sizes can be estimated. Combining the values of ion velocity with the estimated damage sizes, we can understand the changing law of damage size with ion velocity along the ion path. Since the ion velocity at each ion penetration depth can be estimated, the changing law of damage size with the ion penetration depth can be also understood.

TABLE II. The distributions for the ion energy, ion velocity, stopping power, measured columnar defect radius, calculated columnar defect radius, and the damage efficiency (ε) against the ion penetration depth in Fe-irradiated $\text{Bi}_2\text{Sr}_2\text{CaCu}_2\text{O}_x$ crystals.

Depth (μm)	Energy (MeV)	Energy (MeV/amu)	Velocity (c)	dE/dx (keV/nm)	Measured r (nm)	Calculated r (nm)	ε (nm^3/keV)
0	180	3.22	0.083	11.7	1.7	1.55	0.801
1	168	3.01	0.08	11.8	1.7	1.55	0.794
2	156	2.79	0.077	11.9	1.65	1.575	0.742
3	144	2.58	0.074	12.1	1.6	1.575	0.686
4	132	2.36	0.071	12.2	1.6	1.6	0.68
5	120	2.15	0.068	12.3	1.6	1.625	0.675
6	108	1.93	0.064	12.3	1.6	1.625	0.675
7	95.4	1.71	0.061	12.3	1.6	1.625	0.675
8	83.1	1.49	0.056	12.2	1.6	1.65	0.68
9	70.3	1.26	0.052	12	1.55	1.65	0.649
10	59	1.06	0.048	11.8	1.55	1.65	0.66
11	47.4	0.85	0.043	11.3	1.5	1.625	0.645
12	36.4	0.65	0.037	10.7	1.5	1.6	0.682
13	26.6	0.48	0.032	9.67	1.5	1.575	0.754
13.5	22	0.39	0.029	9	1.4	1.425	0.706

It should be mentioned that this method is valid for analyzing the changing law of the damage size along the ion traces. For the quantitative estimation of the damage size in the target materials, however, we still need to solve some problems. First, we have to develop a suitable method to measure the value of D_0 accurately. Also, we still need to improve the method to estimate the $D(r)$ - r curve more accurately.

2. Applications on Au- and Fe- $\text{Bi}_2\text{Sr}_2\text{CaCu}_2\text{O}_x$ irradiation systems

Using the method suggested above, we theoretically analyzed the changing laws of the damage sizes along the ion

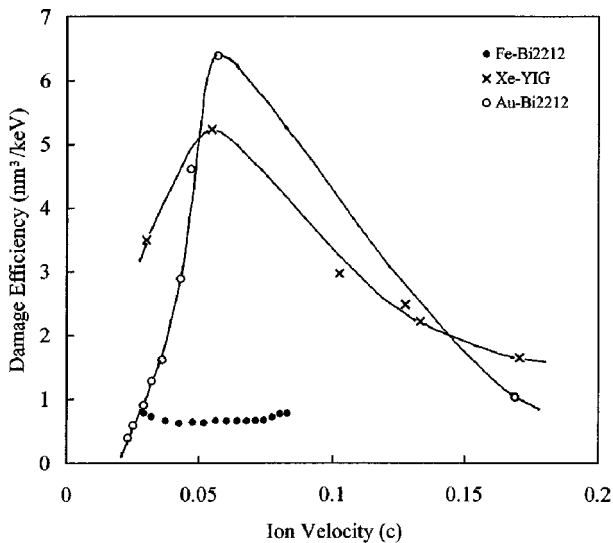


FIG. 4. The velocity dependence of damage efficiency in single ion-target irradiation systems. The solid dots are for Fe- $\text{Bi}_2\text{Sr}_2\text{CaCu}_2\text{O}_x$ irradiation system, the circles for Au- $\text{Bi}_2\text{Sr}_2\text{CaCu}_2\text{O}_x$ irradiation system, and the crosses for Xe-YIG irradiation system. YIG is the yttrium garnet for short. The velocity of light (c) is used as the unit of ion velocity.

traces in both Au- and Fe-irradiated $\text{Bi}_2\text{Sr}_2\text{CaCu}_2\text{O}_x$ crystals. Figures 5 and 6 show two sets of calculated $D(r)$ - r curves in the cases of 230-MeV Au-ion and 180-MeV Fe-ion irradiation, respectively. Looking at the distribution of $D(r)$ - r curves in Fig. 5, for the heavy Au irradiation, all the curves are separated and well ordered by ion energy. For one given value of D_0 , the corresponding values of r_0 is systematically smaller as the ion energy gradually decreases from 200 to 50 MeV along the ion trace. The largest difference of r_0 is about 2 nm. The changing law of the damage size in the theoretic estimation agrees with the experiment results in Ref. 12.

For the light Fe irradiation, however, all the curves are distributed very closely and cross each other (Fig. 6). The

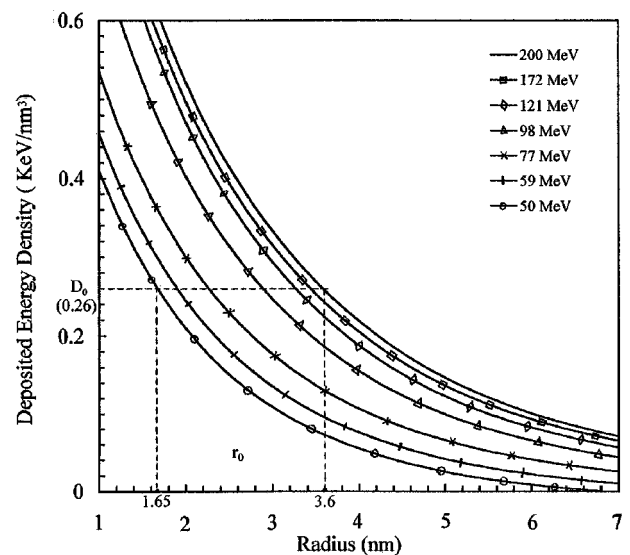


FIG. 5. A series of calculated curves for the radial distribution of the deposited energy density in $\text{Bi}_2\text{Sr}_2\text{CaCu}_2\text{O}_x$ crystal for the Au ions with energies from 200 to 50 MeV. The covered penetration depth region is from 0 to 7.5 μm . All the curves are dispersed in order as ion energy decreases along the ion path.

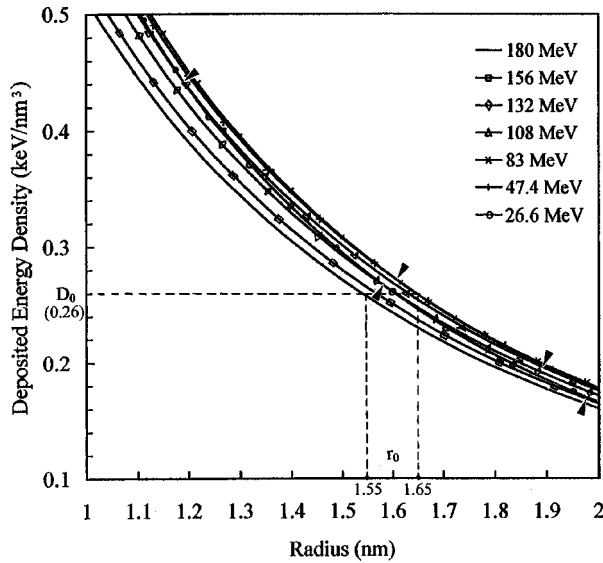


FIG. 6. A series of calculated curves for the radial distribution of the deposited energy density in $\text{Bi}_2\text{Sr}_2\text{CaCu}_2\text{O}_x$ crystal for the Fe ion with energies from 180 to 26.6 MeV. The covered penetration-depth region is from 0 to $13 \mu\text{m}$. All the curves are distributed very closely and crossed each other. The arrow gives the position of each cross point.

corresponding value of r_0 is no longer ordered by the ion energy. For one given value of D_0 , the largest difference of r_0 is only about 0.1 nm, $\frac{1}{20}$ th that in the Au irradiation case. Experimentally, such a small difference of r_0 is hard to detect. Therefore we can approximately take r_0 as a constant. This result implies that the columnar defect size produced by the Fe ion will be a constant, which agrees well with the experiment result shown in this study. The used value of D_0 (0.26 keV/nm^3) in Figs. 5 and 6 is roughly estimated from the experimental data in Fe-ion irradiation. Some error probably exists, but in this study we just use it as a reference for convenience in our discussion.

D. Origin for the formation of the constant columnar defect size

In last section, theoretically, we have identified the possibility for the existence of the long columnar defects with constant columnar size along the ion path in the Fe-irradiated $\text{Bi}_2\text{Sr}_2\text{CaCu}_2\text{O}_x$ crystal. Also, it has been confirmed that this kind of damage morphology is a specific phenomenon in light-ion irradiation, which can never appear in heavy-ion irradiation. Based on this theoretic analysis, here we try to give a brief explanation for how the constant-size columnar defects are produced in light-ion irradiation.

It is known that, for a given target material, dE/dx , ion velocity, and ion effective charge are three changeable factors to decide the evolution of irradiation damage along the ion traces, which are all closely related to the species of incident ion. For the light ion, the lower charge of its nucleus decides that the ion effective charge will be also lower when it moves in the target. Therefore the resistance from the target electrons will be also weaker. This means that the light ion will lose its energy more slowly in the target and the value of dE/dx will be lower, which will further cause dE/dx decreasing more slowly along the ion trace. On the

other hand, if the losing rate of ion-energy is given, the decreasing rate for the ion velocity will be inversely proportional to the ion mass. Therefore, when a lighter ion loses a same amount of energy, the ion velocity will decrease faster.

To sum up, there are two features for the light ion moving in the target: a relative slow decrease of dE/dx and a relative fast decrease of ion velocity along the ion trace. The first feature decides that the distribution of the columnar defect size along the ion trace will be more uniform when a lighter incident ion is used. The second feature indicates that the influence of ion velocity on the $D(r)$ - r curves will be relatively stronger in the light-ion irradiation. In some specific light-ion irradiation system, the slow decrease of the columnar defect size, caused by the slow decrease of dE/dx along the ion trace, can be compensated by the influence of the rapid decrease of ion velocity. This kind of compensation process can be seen from the close and cross distribution of the $D(r)$ - r curves in Fig. 6. Then the long columnar defects with constant columnar size can be observed as in the case of this study. We believe that this kind of specific damage morphology is a general phenomenon, which can be also observed in other kind of light-ion-target irradiation systems.

E. Decrease of dE/dx threshold in light-ion irradiation

To pre-estimate the damage morphology in the target material is very important for all the applications of ion irradiation. Some thresholds for producing different kinds of damage morphologies just provide us with some discriminatory criteria for the correct estimation. One of the well-known thresholds is the dE/dx threshold for generating minimum visible columnar defects in the given target material. It is clear that the detailed value of this dE/dx threshold is closely related to the detailed target material. For example, it needs a very high dE/dx threshold for producing columnar defects in metals. However, for producing columnar defects in insulators and semiconductors, the dE/dx thresholds are much lower.

For $\text{Bi}_2\text{Sr}_2\text{CaCu}_2\text{O}_x$ single crystals in heavy-ion irradiation conditions, the value of the dE/dx threshold has already reported to be $\sim 16 \text{ keV/nm}$.^{12,24,25} Just because the fact that the similar values of dE/dx thresholds were obtained in different kinds of heavy-ion irradiation, people usually take this threshold as a material constant. In this study, we made an attempt at measuring the value of dE/dx in light-ion irradiation. As shown in Fig. 1, we can clearly see the columnar defect existing in the depth region around $13.5 \mu\text{m}$. Combining with the depth profile of stopping power calculated by the extended EDEP-1 code,¹⁵ the threshold of dE/dx in light Fe ion irradiation can be estimated and the detailed value is about 9 keV/nm , which is much lower than the reported value in the case of heavy-ion irradiation. This implies that the dE/dx threshold is not a material constant but related to the incident ion species.

The relation of dE/dx threshold with the incident ion species can be briefly understood as follows. When the incident ion, as a charged particle moving in the target, the energy loss rate (dE/dx) will change with the changes of ion effective charge and ion velocity along the ion trace. For a given value of ion velocity, a heavier ion usually has a higher ion effective charge²⁶ and the energy loss rate (dE/dx) in the

target is also higher. As a result, the produced columnar defect size will be larger. Inversely, for producing a columnar defect with the same size, the required ion velocity will be lower for a heavier incident ion.

According to our previous research results,¹³ in the low-ion velocity region, a lower ion velocity means a lower damage efficiency. Therefore we can further deduce that, for different ion to produce a visible columnar defect with the same size in the same target material, the damage efficiency will be lower for the heavier ion. For example, for producing a columnar defect of 1.4 nm in radius in $\text{Bi}_2\text{Sr}_2\text{CaCu}_2\text{O}_x$ single crystal, the damage efficiency is $\sim 0.706 \text{ nm}^3/\text{keV}$ for Fe ions as shown in Table II but $\sim 0.39 \text{ nm}^3/\text{keV}$ for Au ions.¹³

The dE/dx threshold can be connected with the damage efficiency (ε) through the relation $\varepsilon = A/(dE/dx)$, but here A corresponds to the minimum size of the visible columnar defect produced by incident ion in the target. Since this minimum size of columnar defect is a material constant and free from the change of ion species, the dE/dx threshold will depend inversely as the damage efficiency. As mentioned above, for producing a columnar defect with the same size, the damage efficiency is lower for the heavier ion. Therefore we can further understand that the dE/dx threshold will be higher for the heavier ion in a given target material. From this, we can finally understand why the dE/dx threshold for producing columnar defects is higher for heavy Au ions than for light Fe ions. The detailed analyzing process can be seen elsewhere.²⁷

IV. CONCLUSIONS

The damage behaviors for the high-energy light Fe ions in $\text{Bi}_2\text{Sr}_2\text{CaCu}_2\text{O}_x$ crystals have been investigated by using cross-sectional high-resolution electron microscopy. Differing from the decreasing columnar defect size along the ion path in heavy-ion irradiation, the size of the columnar defect in light Fe ion irradiation can be a constant in a large region of ion penetration depth. Also, the peak of damage efficiency

usually observed in the heavy-ion irradiation does not exist in the light-ion irradiation. In addition, the dE/dx threshold to produce the columnar defect in $\text{Bi}_2\text{Sr}_2\text{CaCu}_2\text{O}_x$ crystals in light Fe-ion irradiation ($\sim 9 \text{ keV/nm}$) is much lower than that in heavy-ion irradiation ($\sim 16 \text{ keV/nm}$).

In order to understand the origins for the appeared specific damage behaviors in light Fe-ion irradiation, a systematic calculation was done for the radial distributions of the deposited energy density, $D(r)$ - r curves, of Fe ions in different penetration depth regions along the ion traces. Then, the required minimum value of deposited energy density to produce permanent damage in the target material (D_0), as a material constant, has been introduced. Combining the calculated $D(r)$ - r curves and the material constant D_0 , a valid method has been suggested to analyze the changing law of the damage size along the ion trace. The applications on Fe- and Au- $\text{Bi}_2\text{Sr}_2\text{CaCu}_2\text{O}_x$ irradiation systems and the obtained results theoretically identified the possibility for the existence of a constant columnar defect size along the ion trace. It has been also confirmed that this kind of phenomenon can only occur in light-ion irradiation and not in heavy-ion irradiation. A qualitative analysis for the threshold of stopping power has also been done and the result proves that the threshold of stopping power is not a material constant but decreases as the mass of incident ion decreases. From this, we can further understand why the threshold of stopping power is lower in light Fe irradiation.

ACKNOWLEDGMENTS

The authors would like to thank Dr. S. Okayasu, Dr. T. Aruga, and Dr. K. Hojou for their kind collaboration in the ion irradiation experiments. This work was partially supported by the New Energy and Industrial Technology Development Organization (NEDO) as Collaborative Research and Development of Fundamental Technologies for Superconductivity Applications.

*Author to whom correspondence should be addressed. Present address: Superconductivity Research Laboratory, ISTE, 2-4-1 Mutsuno, Atsuta, Nagoya 456-8587, Japan. Electronic address: dxhuang@iname.com

¹L. J. Swartzendruber, A. Roitburd, D. L. Kaiser, F. W. Gayle, and L. H. Bennett, Phys. Rev. Lett. **64**, 483 (1990).

²G. Yang, J. S. Abell, and C. E. Gough, IEEE Trans. Appl. Supercond. **3**, 1671 (1993).

³M. V. Feigel'man, V. B. Geshkenbein, A. I. Larkin, and V. M. Vinokur, Phys. Rev. Lett. **63**, 2303 (1989); M. V. Feigel'man and V. M. Vinokur, Phys. Rev. B **41**, 8986 (1990).

⁴G. Blatter, M. V. Feigel'man, V. B. Geshkenbein, A. I. Larkin, and V. M. Vinokur, Rev. Mod. Phys. **66**, 1125 (1994).

⁵L. Civale, A. D. Marwick, T. K. Worthington, M. A. Kirk, J. R. Thompson, L. Krusin-Elbaum, Y. Sun, J. R. Clem, and F. Holtzberg, Phys. Rev. Lett. **67**, 648 (1991).

⁶Terence Hwa, Pierre Le Doussal, David R. Nelson, and Valerii M. Vinokur, Phys. Rev. Lett. **71**, 3545 (1993).

⁷D. R. Nelson and V. M. Vinokur, Phys. Rev. Lett. **68**, 2398 (1992); D. R. Nelson and V. M. Vinokur, Phys. Rev. B **48**, 13 060 (1993).

⁸L. Krusin-Elbaum, A. D. Marwick, R. Wheeler, C. Feild, V. M. Vinokur, G. K. Leaf, and M. Palumbo, Phys. Rev. Lett. **76**, 2563 (1996).

⁹W. Gerhäuser, G. Ries, H. W. Neumüller, S. Schmidt, O. Eibl, G. Saemann-Ischenko, and S. Klaumünzer, Phys. Rev. Lett. **68**, 879 (1992).

¹⁰Y. Zhu, Z. X. Cai, R. C. Budhani, M. Suenaga, and D. O. Welch, Phys. Rev. B **48**, 6436 (1993).

¹¹J. Wiesner, C. Troeholt, J.-G. Wen, H.-W. Zandbergen, G. Wirth, and H. Fuess, Physica C **268**, 161 (1996).

¹²D. X. Huang, Y. Sasaki, S. Okayasu, T. Aruga, K. Hojou, and Y. Ikuhara, Phys. Rev. B **57**, 13 907 (1998).

¹³D. X. Huang, Y. Sasaki, and Y. Ikuhara, Phys. Rev. B **59**, 3862 (1999).

¹⁴Y. Kubo, K. Michishita, Y. Higashida, M. Mizuno, H. Yokoyama, N. Shimizu, E. Inukai, and H. Yoshida, Jpn. J. Appl. Phys., Part 2 **28**, L606 (1989).

¹⁵T. Aruga, K. Nakata, and S. Takamura, Nucl. Instrum. Methods Phys. Res. B **33**, 748 (1988).

¹⁶J. M. Costantini, F. Brisard, J. L. Flament, A. Meftah, M. Toulemonde, and M. Hage-Ali, Nucl. Instrum. Methods Phys. Res. B **65**, 568 (1988).

- ¹⁷J. M. Costantini, F. Ravel, F. Brisard, M. Caput, and C. Cluzean, Nucl. Instrum. Methods Phys. Res. B **80/81**, 1249 (1993).
- ¹⁸A. Meftah, F. Brisard, J. M. Costantini, M. Hage-Ali, J. P. Stoquert, F. Studer, and M. Toulemonde, Phys. Rev. B **48**, 920 (1993).
- ¹⁹F. Studer, C. Houpert, H. Pascard, R. Spohr, J. Vetter, J. Y. Fan, and M. Toulemonde, Radiat. Eff. Defects Solids **116**, 59 (1991).
- ²⁰A. Meftah, N. Merrien, N. Nguyen, F. Studer, H. Pascard, and M. Toulemonde, Nucl. Instrum. Methods Phys. Res. B **59/60**, 605 (1991).
- ²¹F. Studer and M. Toulemonde, Nucl. Instrum. Methods Phys. Res. B **65**, 560 (1992).
- ²²C. X. Zhang, D. E. Dunn, and R. Katz, Radiat. Prot. Dosim. **13**, 215 (1985).
- ²³M. P. R. Waligórski, R. N. Hamm, and R. Katz, Nucl. Tracks Radiat. Meas. **11**, 309 (1986).
- ²⁴M. Leghissa, T. Schuster, W. Gerhäuser, S. Klaumünzer, M. R. Koblichka, H. Kuhn, H.-W. Neumüller, and G. Saemann-Ischenko, Europhys. Lett. **19**, 323 (1992).
- ²⁵H. Kumakura, H. Kitaguchi, K. Togano, H. Maeda, J. Shimoyama, S. Okayasu, and Y. Kazumata, J. Appl. Phys. **74**, 451 (1993).
- ²⁶W. H. Barkas, *Nuclear Research Emulsions—I. Techniques and Theory* (Academic New York, 1963).
- ²⁷D. X. Huang (unpublished).